Available online at website: https://journal.bcrec.id/index.php/bcrec

Bulletin of Chemical Reaction Engineering & Catalysis, 19 (3) 2024, 455-469

Research Article

Investigation on the Hydrothermal Condition in Synthesis of Active Matrix from Metakaolin: Physicochemical Properties and Intrinsic Cracking Activities

Farhansyah Yusuf Putra Hudaya[1], Rezky Oktaviandy Anggaswara[1], Melia Laniwati Gunawan[1,3], Grandprix T. M. Kadja[2,3], I. G. B. N. Makertihartha[1,3*]

[1] Department of Chemical Engineering, Institut Teknologi Bandung, Bandung 40132, Indonesia
[2] Division of Inorganic and Physical Chemistry, Institut Teknologi Bandung, Bandung 40132, Indonesia
[3] Center for Catalysis and Reaction Engineering, Institut Teknologi Bandung, Bandung 40132, Indonesia

Received: 11th July 2024; Revised: 24th August 2024; Accepted: 24th August 2024
Available online: 8th September 2024; Published regularly: October 2024

Abstract

The current trends in research and development of FCC catalyst is focused on the formulation of active matrices that serve as pre-crackers, with the objective of reducing the diffusional resistance of the longer chain hydrocarbon molecule in the feed. In this study, an aluminosilicate active matrix was synthesised from metakaolin using hydrothermal method. The experimental variables that were varied were hydrothermal temperature, in the range of 80 to 110 °C, and hydrothermal time, in the range of 12 to 72 hours, to investigate the best conditions for synthesising the active matrix. Subsequently, the active matrix was subjected to a series of analyses, including X-ray fluorescence, X-ray diffraction, N_2 physisorption, NH_3-temperature programmed desorption, Fourier transform infrared spectroscopy, scanning electron microscopy and thermogravimetry, with the objective of determining its composition, crystal characteristics, surface characteristics, acidity, functional groups, material structure, and thermal characteristics. Additionally, the active matrix was tested for its intrinsic cracking activity using the micro activity test (MAT). The results indicate that the best temperature for hydrothermal synthesis of the active matrix is 80 °C. The active matrix synthesised with a heating time of 24 hours demonstrated the highest light cycle oil yield, reaching 38.9 wt%. Meanwhile, the active matrix synthesised at 48 hours exhibited the most favourable characteristics, with a specific surface area of 144.23 m^2/g and a pore volume of 0.9933 cm^3/g, as well as the highest cracking conversion of 70.0 wt%.

Keywords: Active Matrix; Fluid Catalytic Cracking; Hydrothermal; Metakaolin; Vacuum Gas Oil

How to Cite: F. Y. P. Hudaya, R. O. Anggaswara, M. L. Gunawan, G. T. M. Kadja, I. G. B. N. Makertihartha (2024). Investigation on the Hydrothermal Condition in Synthesis of Active Matrix from Metakaolin: Physicochemical Properties and Intrinsic Cracking Activities. *Bulletin of Chemical Reaction Engineering & Catalysis*, 19 (3), 455-469 (doi: 10.9767/bcrec.20181)

Permalink/DOI: https://doi.org/10.9767/bcrec.20181
Supporting Information: https://journal.bcrec.id/index.php/bcrec/article/downloadSuppFile/20181/5282

1. Introduction

The current global energy demand is still predominantly met by fossil fuels [1]. In 2022, fossil fuels accounted for 23.76% of Indonesia's energy needs, with the majority of this consumption occurring in the transport sector, representing 89.6% of the total. The transport sector is the primary consumer of gasoline (48.7%) and diesel (33.4%) [2]. Gasoline can be produced directly from the distillation process of crude oil. However, the current trend of available crude oil is becoming increasingly heavy, which results in the distillation process producing more heavy oil fractions and residues that must be further treated through the fluid catalytic cracking (FCC) process in order to produce more gasoline [3,4]. The FCC process requires a catalyst composite consisting of zeolite Y as the main cracker, active

* Corresponding Author.
Email: makertia@itb.ac.id (I. G. B. N. Makertihartha)

matrix as the initial cracker, fillers, binders, and additives. The role of the active matrix becomes increasingly important when cracking heavier feeds. Heavy feeds contain long-chain hydrocarbons that are difficult to diffuse to the active sites within the zeolite pore microstructure and thus need to be pre-cracked into shorter ones with the help of the active matrix [5,6].

The active matrix must possess characteristics that are suitable for its function as an initial cracker. In order to facilitate the cracking reaction, the active matrix must contain an adequate number of strong acid sites. An excess of acid sites may result in overcracking, whereas a lacking in acid sites may reduce the cracking conversion [7]. Hydrocarbon molecules in FCC feeds typically have a size of 2.5–10.5 nm, therefore the pore size of the active matrix must be distributed over a larger size range, i.e. macro-mesoporous, for the feed to easily diffuse into the pores [8,9]. Furthermore, the literature indicates that a preferable active matrix should exhibit a specific surface area and pore volume in the range of 350–600 m^2/g and 0.9–1.4 cm^3/g, respectively [10]. An appropriate surface area and pore volume will result in optimal heavy fraction cracking conversion and impurity metal removal [8,11]. In addition to the aforementioned characteristics, a suitable active matrix should exhibit selectivity towards light cycle oil (LCO) products, as these will be further cracked by zeolites into LPG and gasoline [8].

A variety of acidic materials with macro and mesoporous structures have been developed from several bases, including silica-alumina (SA) [10,12–14], γ-alumina [15], and $AlPO_4$ [16]. SA is the most commonly utilised material as an active matrix [17]. In previous studies, the most used alumina source in the synthesis of SA is alumina salts. The resulting SA exhibits a specific surface area in the range of 178–1150 m^2/g and a pore volume in the range of 0.4–1.24 cm^3/g [10,12,14]. Other study has employed kaolin as a green and sustainable alternative source of alumina. The use of a structure directing agent (SDA) silicate-1 enabled the production of SA material from kaolin with a mesoporous structure by hydrothermal method, exhibiting a high surface area up to 545 m^2/g and a pore volume of up to 0.85 cm^3/g [13]. It can be observed that the use of kaolin as an alumina source can also produce ASA with surface characteristics that are not significantly different from those of alumina salts and have the potential to be used as an active matrix. However, the SA has not been tested for its intrinsic cracking activity [13].

In this study, SA-based active matrices were synthesised using a hydrothermal method with metakaolin and fumed silica precursors. The objective was to investigate the best hydrothermal synthesis parameters to produce suitable physiochemical properties and intrinsic cracking activity of the active matrix, as previously stated, without the use of SDA. The first variable to be investigated was the hydrothermal temperature, followed by the hydrothermal time. An Si/Al molar ratio of 10 was used, which is the value for achieving the highest LCO yield, as evidenced in the literature [14]. Furthermore, 1 wt% phosphorus was also added to enhance the hydrothermal stability and pore diameter of the active matrix [10,11].

2. Materials and Methods

2.1 Active Matrix Synthesis

An active matrix with a Si/Al molar ratio of 10.0 and a phosphorus content of 1.0 wt% was prepared, using a hydrothermal method described in the literature [13]. The synthesis process started by preparing metakaolin by calcining kaolin at 700 °C for 7 hours. The metakaolin was then mixed with NaOH (Merck 99%) that has been dissolved in aqua dm. Fumed silica (HJSIL 200) was added under continuous stirring to obtain a homogeneous gel with molar composition of 10 Na_2O:100 SiO_2:5 Al_2O_3:1800 H_2O. A solution of H_3PO_4 (Merck, 85 wt%) was then added to the gel and stirred until homogenised.

The mixture was then heated in a teflon lined stainless steel autoclave at temperatures 80 to 110 °C for a period of 12 to 72 hours, after which it was cooled at a slow rate for a period of one day. The resulting solid was then washed to a pH of 8, dried, and calcined at a temperature of 550 °C for a period of six hours. The synthesised active matrix was named SAM-TXX-JYY, with XX denoting the hydrothermal temperature and YY denoting the hydrothermal time.

2.2. Characterizations

The composition of metakaolin and active matrices was analysed by X-ray Fluorescence (XRF) using a Rigaku NEX CG serial CG1544 instrument with a helium atmosphere. The crystallinity of kaolin, metakaolin and the active matrix was analysed using a Bruker D2 PHASER X-ray Difractometer (XRD) at 2θ of 5–70°. The specific surface area, pore volume, average pore diameter, and pore size distribution were analysed by the N_2-physisorption method using a Micromeritics® Tristar II Plus 3.01 instrument. The acidity was analysed using the NH_3-TPD (NH_3-Temperature Programmed Desorption) method on a BELCAT II instrument. The thermal properties was determined based on the thermogravimetric method with a LINSEIS STA Platinum Series instrument in the temperature range of 30–1000 °C and an air atmosphere. Infrared spectra of the active matrix and

metakaolin were analysed using a Bruker ALPHA FTIR (Fourier Transform Infrared) instrument at wavelengths of 500–4000 cm^{-1}. The surface morphology of the active matrices was captured using a scanning electron microscope (SEM), specifically the Hitachi SEM SU3500 instrument.

2.3. Cracking Activity Test

The intrinsic cracking activity of active matrices was tested using Micro Activity Test (MAT) method according on the TEXOL Fixed Bed Micro Reactor Unit with serial number 3210-200-10-12. The operating conditions were selected in accordance with the standard set forth in ASTM D5154-03 and ASTM D3907-03. A total of 4 grams of active matrix sample was used to crack 1.36 grams vacuum gas oil (VGO) feed over a feeding time period of 76 s, resulting in a weight hourly space velocity (WHSV) of 16.1 h^{-1}. The reaction temperature employed is the standard MAT testing temperature, which is 516 °C. A cooling water is used to condense the cracking products. A condenser was used to collect the liquid product while a gas sampling bag collected the gas product. The spent active matrix was also collected to be analysed by themogravimetric method.

2.4. Cracking Product Analysis

The mass of the gas product was determined based on the mass balance, assuming that no mass was lost or gained during the reaction and measurement process. The yield of gas was determined using Equation (1). The composition of the product gas was analysed using the GC (gas chromatography) method. To analyse the gas composition of H_2, CO, CO_2, and CH_4, a Perkin-Elmer GC with thermal conductivity detector and RT® Msieve 5A and PorapakTM Q columns was used. The device programmed to analyse at 90 °C. To analyse the C_1–C_4 gases, a Shimadzu GC-2014 with a flame ionisation detector and an RT® Alumina BOND/Na_2SO_4 column was used. The device programmed to analyse from 28 to 197 °C with heating rate of 21 °C/minute.

$$Y_{gas} = 1 - Y_{OLP} - Y_{coke} \quad (1)$$

The yield of the organic liquid product (OLP) was determined by weighing, while the composition was analysed using simulated distillation gas chromatography on an Agilent Technologies 7890B instrument with a flame ionisation detector in accordance with ASTM D2887. The device programmed to analyse from 40 to 524 °C with heating rate of 1 °C/s. The reference boiling points employed in the determination of the liquid product types were those of gasoline, ranging from 30 to 215 °C; light cycle oil (LCO), ranging from 216 to 390 °C; and heavy cycle oil (HCO), above 390 °C. The yield of the OLP (Y_{OLP}), gasoline fraction ($Y_{gasoline}$), diesel fraction (Y_{LCO}), and HCO fraction (Y_{HCO}) was determined using Equation (1) to Equation (4).

$$Y_{OLP} = \frac{mass\ of\ OLP}{mass\ of\ VGO\ feed} \quad (2)$$

$$Y_{gasoline} = \frac{mass\ of\ gasoline\ fraction}{mass\ of\ VGO\ feed} \quad (3)$$

$$Y_{LCO} = \frac{mass\ of\ LCO\ fraction}{mass\ of\ VGO\ feed} \quad (4)$$

$$Y_{HCO} = \frac{mass\ of\ HCO\ fraction}{mass\ of\ VGO\ feed} \quad (5)$$

The conversion (X_{VGO}) was determined on the assumption that the HCO fraction was the reactant that was not cracked by the active matrix. The conversion (X) and activity of the active matrix was determined by means of Equation (5) and Equation (6), respectively.

$$X_{VGO} = 1 - Y_{HCO} \quad (6)$$

$$Activity = \frac{Conversion}{1 - Conversion} \quad (7)$$

The coke, water content, and light hydrocarbon compounds in the surface of spent matrix were analyzed using the thermogravimetric method. The samples were heated to 100 °C to analyse the water and light hydrocarbon content. Subsequently, the samples were calcined at 700 °C to analyze the formed coke yield. The yield of coke (Y_{coke}) was determined by means of Equation (7).

$$Y_{coke} = \frac{mass\ of\ coke}{mass\ of\ VGO\ feed} \quad (8)$$

3. Results and Discussion

3.1. Metakaolin Composition

The oxide compound composition of metakaolin, obtained from the calcination of

Table 1. Composition of metakaolin which was analyzed by XRF

Component	Composition (wt%)
K_2O	0.42
TiO_2	0.40
Fe_2O_3	0.86
Al_2O_3	39.00
SiO_2	55.90
Others	3.42

kaolin, is presented in Table 1. The others are the components that were not identified by the XRF instrument.

3.2. Active Matrix Characteristic

X-ray diffraction was used to analyze the crystallinity of the kaolin, metakaolin, and active matrix samples. The diffractogram in Figure 1 shows that the kaolin material initially had a crystalline structure, but after being heated at high temperature, the crystalline kaolinite structure changed to amorphous (metakaolin) with some quartz peaks still present. The SAM-T80-J48 active matrix, synthesized from metakaolin, also contains an amorphous silica-alumina phase, as indicated by the presence of a large hump at 2θ = 10–40°, similar to the findings of previous research [13,18]. However, the metakaolin and SAM-T80-J48 sample still contain a crystalline quartz phase, as indicated by the sharp diffraction peak at 2θ = 26.6°. The amorphous structure of SAM-T110-J24, SAM-T80-J24, SAMP-T80-J48 are also shown by the SEM image on Figure 2. Figure 2 also illustrate the formation of agglomerate structure in the three sample, as observed in the previous research [13].

Surface characteristic and number of acid sites of kaolin, metakaolin, and active matrices are presented in Table 2. All the samples exhibited actual Si/Al ratio values between 8–10.1, which is close to the target value of 10 during synthesis. Regarding the surface characteristic, all sample have met the target average pore diameter and SAM-T80-J48 has met the specified target for mesopore volume. However, none of the samples have reached the target specific surface area, as desired. The highest surface area is observed in SAM-T80-J48, that is 144.23 m^2/g.

In each active matrix sample, there was an increase in surface area, pore volume, pore diameter, and number of acid sites compared to the precursor, metakaolin. This indicates that the

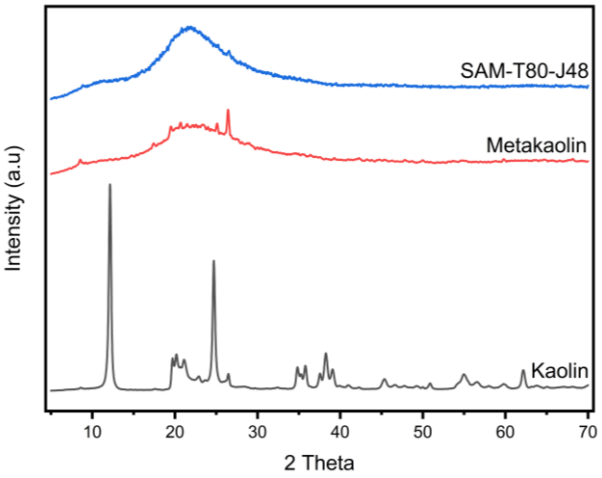

Figure 1. Diffractogram of kaolin, metakaolin, and SAM-T80-J48

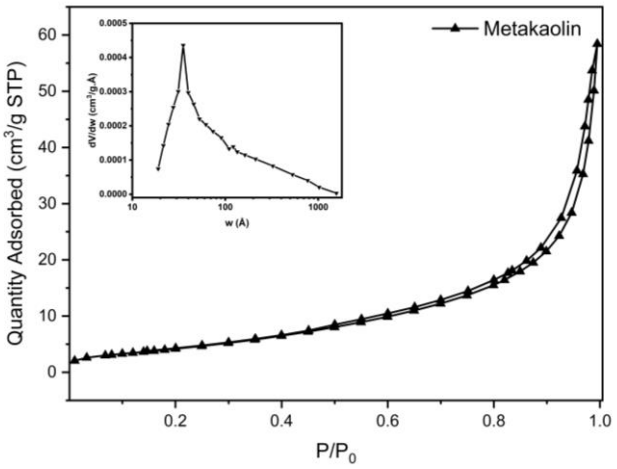

Figure 3. N_2 adsorption/desorption isotherm and pore size distribution of metakaolin

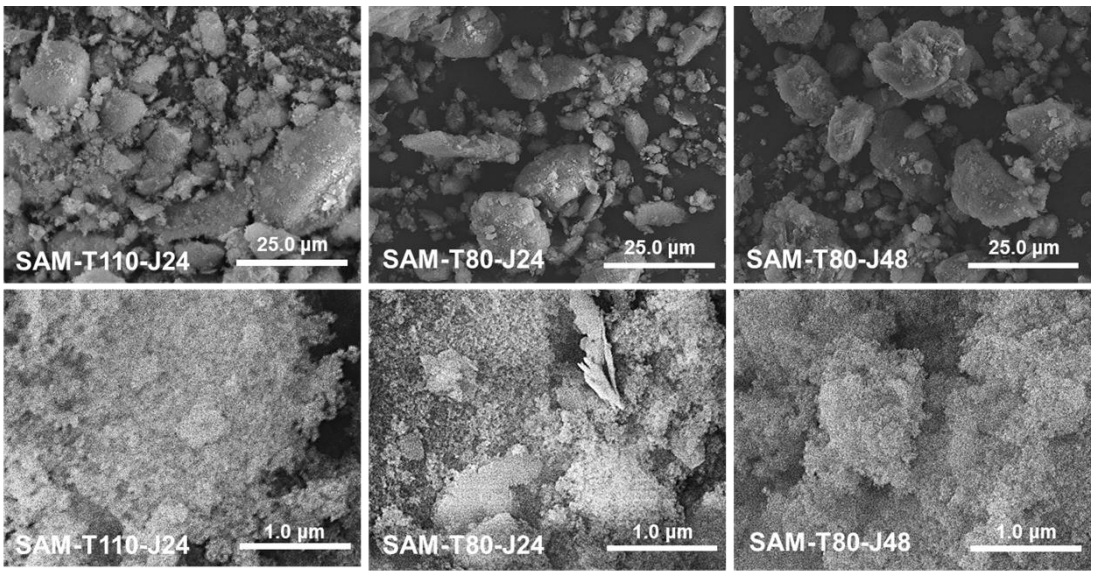

Figure 2. SEM image of SAM-T110-J24, SAM-T80-J24, and SAM-T80-J48

structure of metakaolin undergoes a transformation when processed into an active matrix. Figure 3 illustrates that the initial metakaolin sample exhibits a Type III adsorption isotherm pattern, indicating that the material is non-porous or contains macropores [19]. However, the porous distribution curve indicates that the metakaolin sample has only a few micropores with a small volume, suggesting that it may have no pores. Upon becoming an active matrix, the resulting isotherm transitions to type V, as illustrated in Figure 4 and Figure 5. This indicates the formation of new mesopores. Furthermore, samples of SAM-T80-J24, SAM-T80-J36, and SAM-T80-J48 exhibit H1-type hysteresis, indicating that the three samples contain pores with a relatively uniform shape and size [20,21]. In the remaining samples, H2(b) type hysteresis is formed, indicating that pore blockage occurs during the desorption process. This is because the pores in the remaining samples have different sizes of pore mouths and bodies, although the size difference is not too large. This is in accordance with the findings of [21,22].

Acidity is a crucial property for the active matrix, which acts as the initial cracker in FCC catalyst composites [23]. The results of the NH_3-TPD analysis revealed that the number of acid sites in metakaolin increased from 0.017 mmol NH_3/g to 0.174–0.244 mmol NH_3/g after processing into active matrix. This increase in acidity was attributed to the formation of new acidic pores in the material [24]. Furthermore, the NH_3-TPD curve in Figure 6 reveals the presence of two peaks at 100–250 °C and 550–800 °C, which indicate the existence of two distinct levels of acid site strength in the sample [25]. The weak acid sites indicated by the initial peak are involved in carrying out secondary reactions, including isomerisation, cyclisation, and hydrogen transfer.

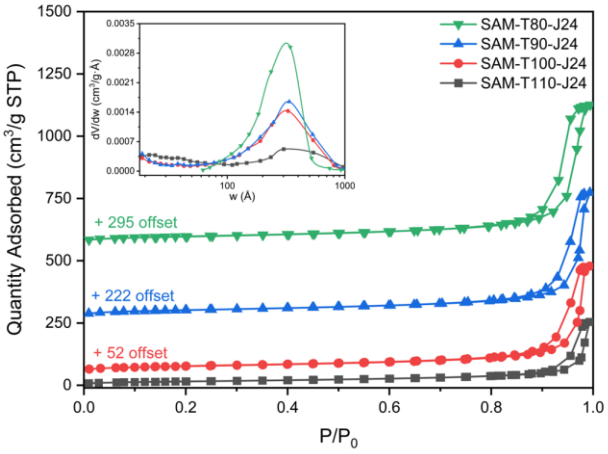

Figure 4. N_2 adsorption-desorption isotherm and BJH desorption pore size distribution of active matrices with variation of hydrothermal temperature and Si/Al ratio = 10

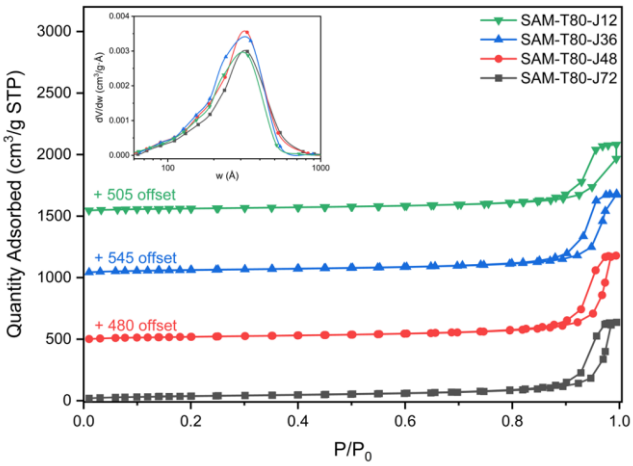

Figure 5. N_2 adsorption-desorption isotherm and BJH desorption pore size distribution of active matrices with variation of hydrothermal time and Si/Al ratio = 10

Table 2. Si/Al molar ratio, surface characteristic, and acidity of active matrices

Sample name	Si/Al molar ratio	Specific surface area (m^2/g)	Specific mesopore volume (cm^3/g)	Average pore diameter (Å)	Number of acid site (mmol NH_3/g)		
					Weak acid	Strong acid	Total
Kaolin	-	17.58	0.0630	116.54	-	-	-
Metakaolin	-	16.80	0.0656	156.12	0.007	0.010	0.017
SAM-T80-J24	8.20	108.64	0.8009	281.44	0.045	0.198	0.243
SAM-T90-J24	10.09	102.27	0.6269	307.34	0.022	0.152	0.174
SAM-T100-J24	7.95	91.52	0.5665	294.12	0.050	0.141	0.191
SAM-T110-J24	7.95	57.82	0.2174	275.67	0.061	0.125	0.186
SAM-T80-J12	10.01	124.62	0.8548	270.62	0.026	0.186	0.212
SAM-T80-J36	9.81	138.36	0.8765	278.32	0.034	0.210	0.244
SAM-T80-J48	9.80	144.23	0.9933	292.92	0.038	0.188	0.226
SAM-T80-J72	9.45	133.04	0.8554	300.19	N/A	N/A	N/A
Target	10	350-600	0.9-1.4	>50	-	-	-

In contrast, the strong acid sites observed in the second peak are crucial for the execution of cracking reactions [7]. In line with its role as an initial cracker, the active matrix should exhibit a greater prevalence of strong acid sites than weak acid sites.

Figure 7 shows the infrared spectra of the metakaolin and SAM-T80-J24 samples. Several spectral peaks are observed at wavelengths of 801, 1067, 1505, 1696, 2366, and 3745 cm^{-1}. Infrared vibrations at wavelengths of 801 and 1067 cm^{-1} indicate the presence of symmetric and asymmetric structures of tetrahedral AlO_4 and SiO_4 that form Si–O–Al and Si–O–Si bonds, respectively [13,26,27]. Vibrations around 1660 cm^{-1} indicate the presence of water (H–O–H bonds) adsorbed in the material [27,28]. In addition, after metakaolin is converted into an active matrix, it can also be observed that there is a broadening and increase in the vibrational intensity at 1067 cm^{-1}. This indicates the formation of new asymmetric Si–O–Al bonds in the active matrix [29].

Figure 8 shows thermogravimetric analysis results for kaolin, metakaolin, and SAM-T80-J48. It can be observed that the mass of the material changes at different temperatures. From room temperature to 170 °C, the mass slightly decreases due to evaporating free water contained in the material. Then, there is also a slight decrease in mass at 170–250 °C due to the evaporation of interstitial and hydrates water [30]. Slight increase and decrease in mass at 300–475 °C may be due to dehydroxylation or phase change of amorphous Fe_2O_3 to crystalline [31–33]. A decrease in mass occurs at 475–600 °C due dehydroxylation reactions in the compounds contained in the samples. The higher mass decrease in kaolin is due to the dehydroxylation of kaolinite phase which transformed into metakaolinite phase [26,34]. At temperatures 850–1000 °C, further mass decrease occurred due to phase changes and degradation of compound in the material [33,35].

3.3. Hydrothermal Temperature Effect on Matrix Characteristic

The surface characteristics of the active matrix are affected by hydrothermal temperature. Figures 9 demonstrate the correlation of hydrothermal temperature on specific surface area and specific mesopore volume. Figure 9 (A) indicates that the best temperature to synthesize active matrix from metakaolin is 80 °C. It can be observed that an increase in the hydrothermal temperature is associated with a reduction in both the surface area and pore volume. The decrease is particularly pronounced at temperatures above the normal boiling point of water (approximately 100 °C), due to the formation of steam that catalyses the dealumination reaction. Dealumination is the hydrolysis of aluminum in the Si–OH–Al bond (bond angle 145.95), which

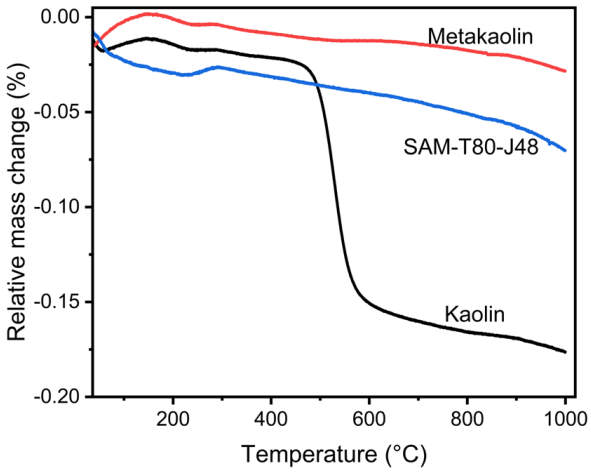

Figure 8. Thermogravimetric analysis of kaolin, metakaolin, and SAM-T80-J48

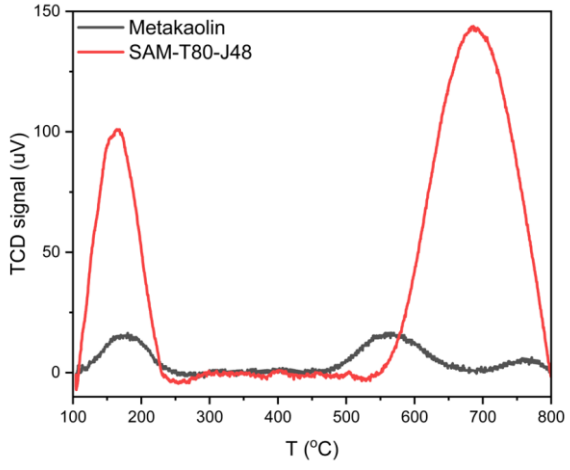

Figure 6. NH_3-TPD curve of metakaolin and SAM-T80-J48

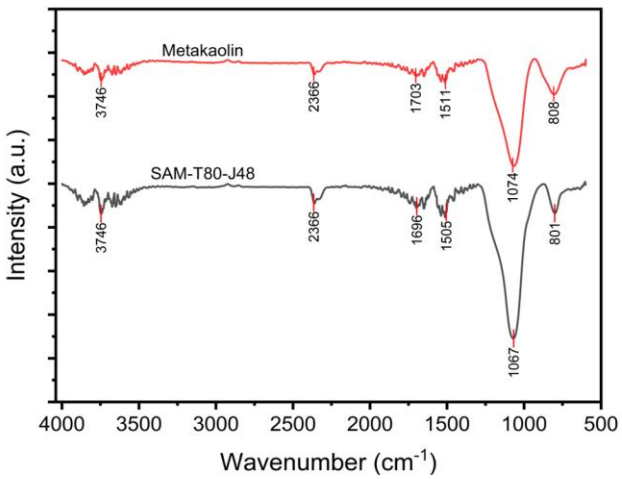

Figure 7. Infrared spectra of metakaolin and SAM-T80-J24

produces Si–OH bonds (length 1.59 Å). As a consequence of the dealumination process, the number of Al–O bond (length 1.71 Å) is decreasing, resulting in pore shrinkage which has an impact on the decrease in surface area [18,36]. Furthermore, hydroxide ions that present act as catalysts for the densification process, which is the formation of siloxane (Si–O–Si) bonds from the condensation process of silanol (Si–OH) groups. At higher temperatures, the kinetics of the dealumination and densification reactions will become faster, resulting in a decrease in pore volume [37].

Table 3 present the pore size distribution analysis of the samples at various hydrothermal temperatures. The data suggests that the number of small (<100 Å) and large (> 450 Å) pores increases as the hydrothermal temperature rises. This phenomenon occurred likely due to the rapid densification, hydrolysis, and cross-linking processes that occur at high temperatures, resulting in more water being trapped in the pore frame of the material. When water is removed, a larger pore structure is formed [37,38]. Additionally, it is observed that at lower hydrothermal temperatures, the resulting pore size distribution is more uniform than at higher temperatures. The SAM-T80-J24 sample has a more uniform pore size distribution, with pore sizes mostly in the range of 200–450 Å, compared to the other samples. This can influence the selectivity of cracking. Moreover, the active matrix must be designed to have meso-macro pores to facilitate the diffusion of long-chain hydrocarbons into the zeolite [7].

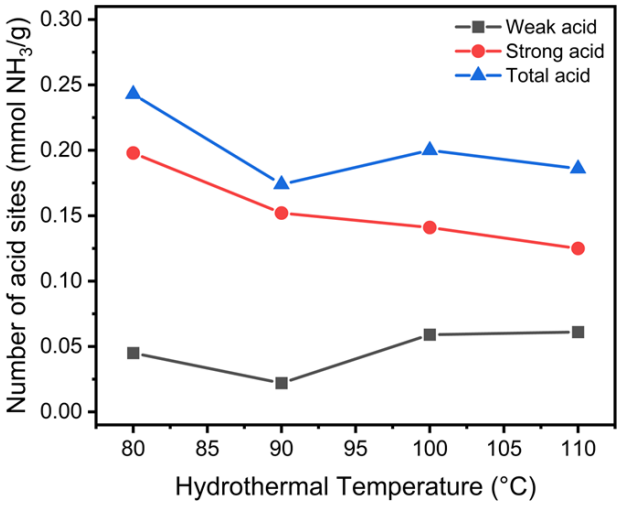

Figure 10. Effect of hydrothermal temperature on number of acid sites in the synthesized active matrix with Si/Al molar ratio of 10 and hydrothermal time.

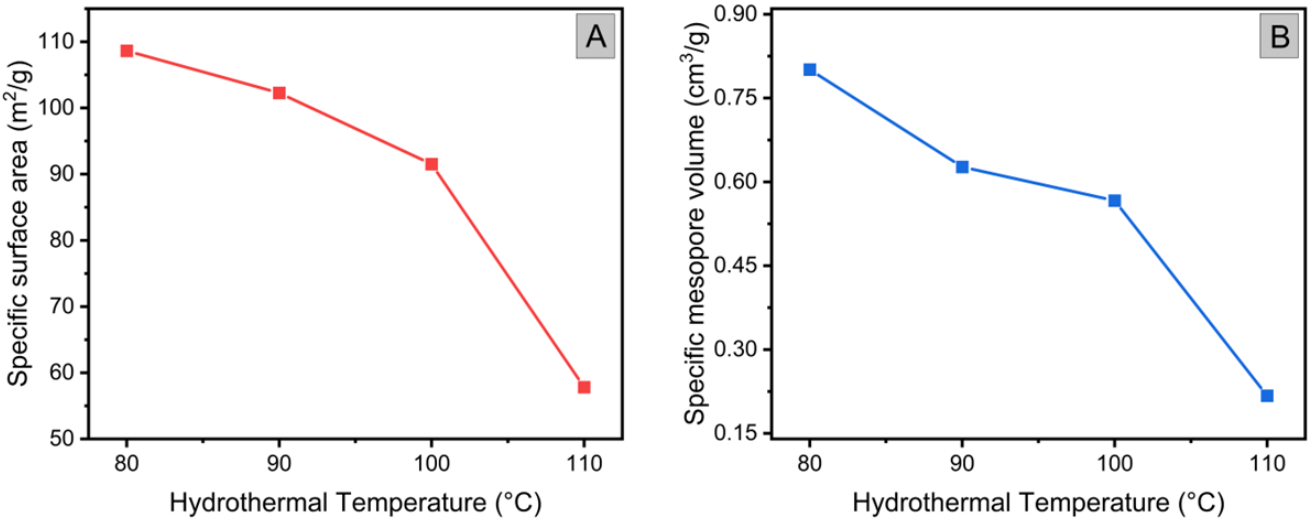

Figure 9. Effect of hydrothermal temperature on (A) specific surface area and (B) specific mesopore volume of synthesized active matrix with Si/Al molar ratio of 10 and hydrothermal time of 24 hours

Table 3. Pore size distribution of synthesized matrices with varied hydrothermal temperature, Si/Al molar ratio of 10, and hydrothermal time of 24 h

Pore size range (Å)	Pore size distribution (%)			
	SAM-T80-J24	SAM-T90-J24	SAM-T100-J24	SAM-T110-J24
< 100	0.7	2.4	2.5	5.2
100–200	11.0	9.0	9.0	5.9
200–450	77.0	44.2	49.5	29.0
450–1000	10.3	43.4	37.9	55.0
> 1000	1.0	1.0	1.1	4.9

Figure 10 illustrates the relationship between the number of acid sites (weak, strong, and total) and hydrothermal temperature at a Si/Al molar ratio of 10 and a 24-hour hydrothermal time. A fluctuating correlation was observed, with the number of acid sites demonstrating minimal variation at varying hydrothermal temperatures. This could be attributed to the complex, amorphous, non-ordered structure of the active matrices, which did not allow for a precise relationship to be established with a single variation. However, the sample treated at the hydrothermal temperature of 80 °C was selected for further investigation as it exhibited the highest number of acid sites among all tested samples.

3.4. Hydrothermal Time Effect on Matrix Characteristic

Upon obtainment of the best hydrothermal temperature of 80 °C, the active matrix was then synthesised with varying hydrothermal times. Based on Figures 11, it can be concluded that the surface area and pore volume of the active matrix increased as the hydrothermal time increased from 24 to 48 hours and then decreased at heating time exceeding 48 hours. The phenomenon of increasing surface area and pore volume with increasing hydrothermal time up to 48 hours was also reported by previous research [13]. This phenomenon can be attributed to the condensation reactions of silanol groups (Si–OH) occurring at hydrothermal times up to 48 hours, which result in the formation of a better mesoporous structure [13,39]. The reduction in specific surface area and mesopore volume can be attributed to the higher degree of densification reaction that results from longer hydrothermal

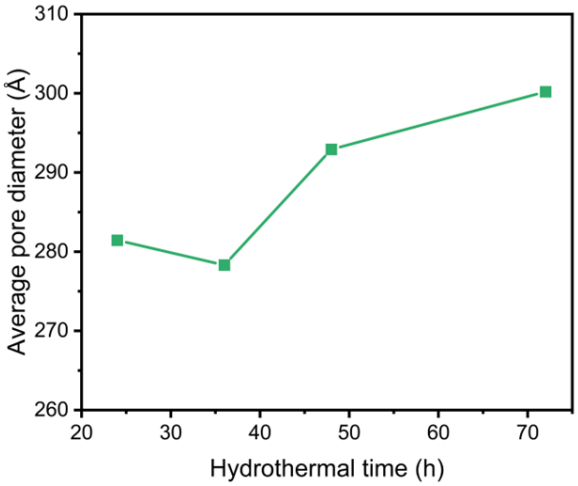

Figure 12. Effect of hydrothermal time on average pore diameter of synthesized active matrix with Si/Al molar ratio of 10 and hydrothermal temperature of 80 °C

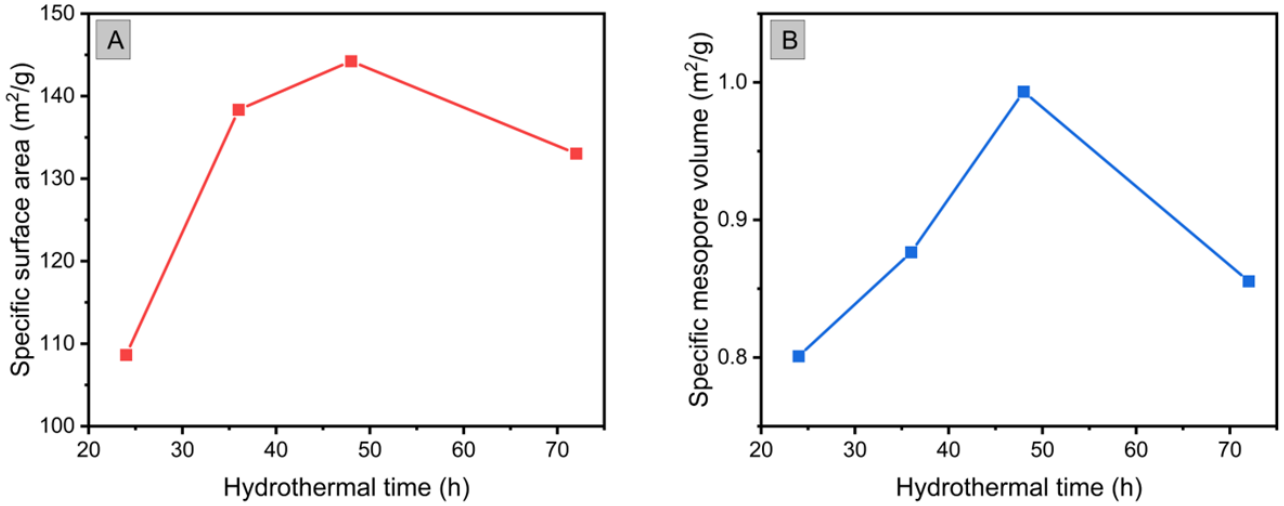

Figure 11. Effect of time on (A) specific surface area and (B) specific mesopore volume of synthesized active matrix with Si/Al molar ratio of 10 and hydrothermal temperature of 80 °C

Table 4. Pore size distribution of synthesized matrices with varied hydrothermal time, Si/Al molar ratio of 10, and hydrothermal temperature of 80 °C

Pore size range (Å)	Pore size distribution (%)			
	SAM-T80-J12	SAM-T80-J36	SAM-T80-J48	SAM-T80-J72
< 100	1.2	1.1	1.0	0.8
100–200	11.6	12.0	10.6	9.1
200–450	78.8	77.3	69.1	70.5
450–1000	7.3	8.8	18.6	18.8
> 1000	1.0	0.8	0.7	0.8

times [37]. From Figures 10, it can be observed that the best hydrothermal time for the synthesis of an active matrix from metakaolin is 48 hours.

According to Figure 12, the average pore diameter tends to increase as the hydrothermal time increases. Table 4 shows that the active matrix synthesized with a hydrothermal time of 48 and 72 hours has more pores with sizes ranging from 450 to 1000 Å. It can also be observed that on heating time up to 48 hours, there is an increase in pore volume, as evidenced by the higher peak of the BJH curve in Figure 5. This demonstrates that longer hydrothermal times result in the formation of more pores with larger sizes. Therefore, the surface area increases as well, even though the average pore diameter increases. This phenomenon is consistent with the findings of previous research [13]. The previous study also showed that longer hydrothermal times, particularly until 48 hours, result in increased material porosity and the formation of additional macro pore structures, resulting in bimodal meso-macro pore porosity, which is necessary for active matrix as initial cracker [8,40].

Figure 13 illustrates the correlation between the number of acid sites (weak, strong, and total)

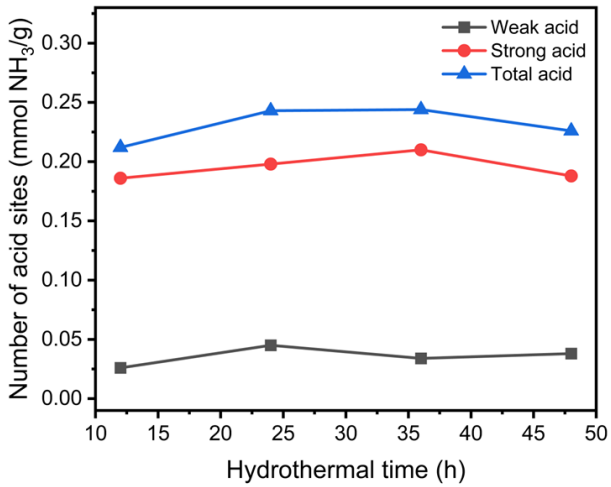

Figure 13. Correlation of hydrothermal time to the number of acid sites in the synthesized active matrix with Si/Al molar ratio of 10 and hydrothermal temperature of 80 ^{0}C.

and the hydrothermal time at a Si/Al molar ratio of 10 and an 80 °C hydrothermal temperature. It was observed that the number of acid sites did not undergo a significant change as the hydrothermal time was varied. As previously stated, this could be attributed to the complex, amorphous, non-ordered structure of the active matrices, whereby a single variation did not provide an exact relationship. Consequently, the active matrix cracking activity can be indirectly influenced by its pore size distribution. A suitable pore size distribution can facilitate the diffusion of large hydrocarbon molecules to the acid sites in the pore, thus the cracking activity will increase [41].

3.5. Cracking Performance

The cracking performance of synthesised active matrices were examined using the Micro Activity Test (MAT). Table 5. summarises the VGO cracking products for each sample. The term OLP is an abbreviation for organic liquid product. According to Table 5, the conversions were quite varied, ranging from 58.2 to 70.0%. Raising the hydrothermal temperature had no significant effect on the active matrix cracking activity, despite the catalytic activity increases at temperatures above 110 °C. Furthermore, as the hydrothermal time increase, the catalytic activity also increases. The highest catalytic activity was observed in the SAM-T80-J48 sample, specifically 2.33.

The catalytic activity is proportional to the number of strong acid sites present in the active matrix. As the number of strong acid sites present in the active matrix increases, the catalytic activity also increases [7,8]. However, it is notable that certain samples in this study exhibited behavior that did not align with the aforementioned theory. The number of strong acid sites in SAM-T80-J48 is less than that in SAM-T80-J36, yet the catalytic activity is greater. This could be attributed to the other characteristics of SAM-T80-J48, including a relatively larger surface area and pore volume. The extensive pore volume facilitates a more efficient hydrocarbon

Table 5. Active matrices cracking activity and cracking product analysis

Parameter	SAM-T80-J24	SAM-T90-J24	SAM-T100-J24	SAM-T110-J24	SAM-T80-J12	SAM-T80-J36	SAM-T80-J48
Conversion (%)	58.8	59.6	58.2	62.5	63.5	69.1	70.0
Gas product yield (%)	10.1	18.3	14.4	20.3	19.7	26.3	1.5
OLP yield (%)	88.7	80.1	84.3	78.7	76.9	69.7	97.2
Gasoline yield (%)	8.5	7.4	7.0	8.8	7.9	7.4	35.2
LCO yield (%)	38.9	32.4	35.6	32.4	32.6	31.4	32.0
HCO yield (%)	41.2	40.4	41.8	37.5	36.5	30.9	30.0
Coke yield (%)	1.2	1.6	1.3	0.9	3.4	4.0	1.2
Activity	1.42	1.48	1.39	1.66	1.74	2.23	2.33

diffusion process. With such a large pore volume and surface area, the cracking of heavy hydrocarbons can occur more effectively, resulting in a higher cracking activity [8,42].

3.5.1 Gas product

Gas Chromatography (GC) with FID and TCD detectors was used to analyze the cracking gas products. The chromatogram of the gas cracking products of SAM-T80-J48 that was analysed by FID GC is illustrated in Figure 14. It can be seen that the identified hydrocarbon gas products from the FID GC analysis were ethane, propane, propylene, isobutane, n-butane, isobutylene, cis 2-butene, 1,3 butadiene, n-pentane, isopentane and a small fraction of light gasoline. Additionally, the predominant hydrocarbon gas present in the cracking product of SAM-T80-J48 is propylene, as determined through chromatogram peak area analysis. The TCD GC analysis results shows that the cracking gas products contain high amount of CO_2 and H_2 gas. Further details regarding the GC responses for gaseous products can be found in Tables S1 and S2, which can be accessed in Supporting Information.

3.5.2 Organic liquid product

The results of simulated distillation GC analysis, as presented in Table 5, indicate that the LCO yield for all active matrix exceeds the targeted value of 30 wt%. The highest LCO yield was exhibited by SAM-T80-J24 sample, specifically 38.9 wt%. The high selectivity of LCO products in this sample is attributed to their more uniform porous size distribution within the 200–450 Å range, in comparison to other hydrothermal temperature variation samples. In addition, the HCO yield decreased as the hydrothermal time of the active matrix increased, followed by a decrease in LCO yield and increase in gasoline yield, even though the acidity was not significantly different. This phenomenon occurs because the sample synthesizes with longer the heating time has higher specific surface area and mesopore volume, thus the cracking activity increases [7,8,43]. In addition, bimodal porosity (mesopores and macropores) can also affect the cracking conversion. In materials with bimodal porosity, the surface area on the smaller pores can interact rapidly with the feed due to the faster diffusion process facilitated by the larger pores [40,44].

3.5.3 Coke content

Table 5 indicates that each active matrix sample has met the coke yield target, which is below 5 wt%. It can be seen that coke yield tends to decrease as the hydrothermal temperature increases during the active matrix synthesis process. This phenomenon can be attributed to the fact that at elevated hydrothermal temperatures, the number of strong acid sites, which play a role in the cracking reaction, is reduced. The relatively larger number of strong acid sites in SAM-T90-J24 results in a higher coke yield due to overcracking phenomenon [8,45].

The hydrothermal time does not appear to have an impact on coke yield, as there is no discernible correlation between the two variables.

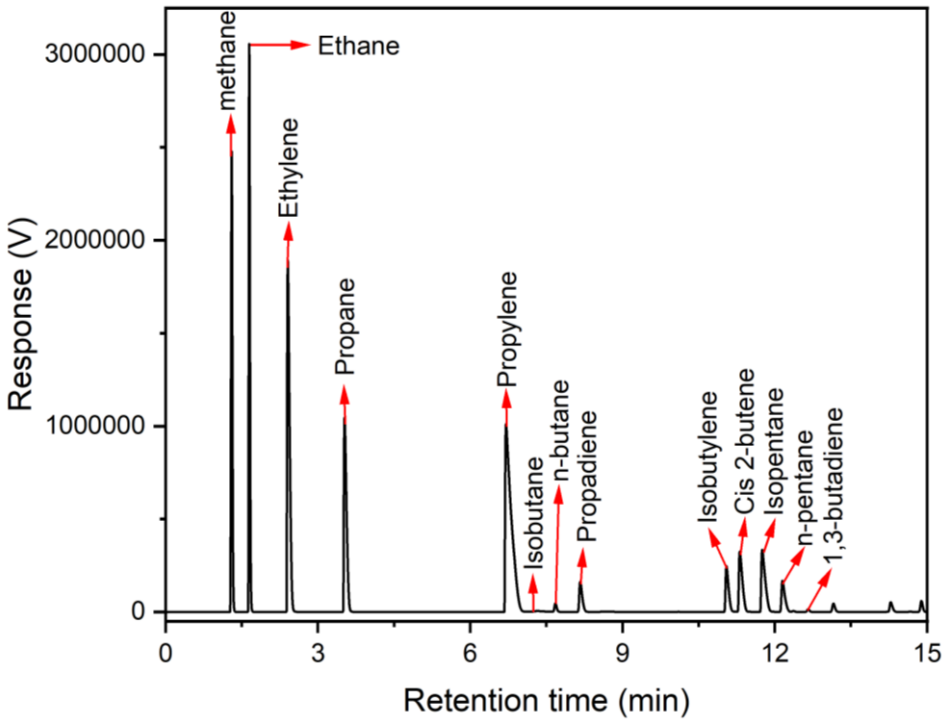

Figure 14. Chromatogram of gas cracking product of SAM-T80-J48 that was analysed by FID GC

According to Table 5, it can be seen that the cracking activity increases in the following order: SAM-T80-J24 < SAM-T80-J12 < SAM-T80-J36 < SAM-T80-J48. This suggests that coke yield should also increase in this order, because coke yield should be primarily influenced by catalytic activity [8,45]. However, the coke yield increased in the following order instead: SAM-T80-J24 = SAM-T80-J48 < SAM-T80-J12 < SAM-T80-J36. The low coke yield with high activity in sample SAM-T80-J48 may be influenced by the presence of numerous macroporous structures in the sample. Thus, it allows hydrocarbon particles that undergo cyclisation, isomerization, and alkylation in the active matrix pores to easily diffuse out of the pores, preventing repeated cracking that can lead to overcracking [46–48].

4. Conclusion

Amorphous SA-based active matrix was successfully synthesised from metakaolin without the use of SDA. The surface characteristics of the resulting SA are not as good as those of SA synthesised from kaolin using SDA. However, it still has the potential to be used as an active matrix due to its acidic properties and macro-mesoporous structure. The resulting specific surface area is still below the desired value for an active matrix, but the resulting pore volume has reached the desired value. Further study and development are required to achieve each desired characteristic.

The investigation of synthesis parameter result indicates that the higher hydrothermal temperatures lead to a decrease in surface area, pore volume, acidity, average pore diameter, coke yield, and LCO recovery. Additionally, longer hydrothermal time tend to increase surface area, pore volume, average pore diameter, and cracking conversion. However, when the hydrothermal time exceeded 24 hours, the LCO yield decreased while the gasoline and gas product yield increased. Therefore, the best hydrothermal temperature was determined to be 80 °C, with a hydrothermal time of 24 hours for high LCO yield of 38.9 wt% and 48 hours for high surface area of 144.23 m^2/g, high pore volume of 0.9933 cm^3/g, and high conversion of 70.0%.

Acknowledgements

This research is supported and funded by RU3P-2024 LPIT-ITB (grant number LPIT1.PN-6-38-2024) and P2MI-Faculty of Industrial Technology-ITB (grant number PPMI-1-61-2024).

CRediT Author Statement

Author Contribution: F.Y.P. Hudaya: writing-original draft, investigation, data curation, visualization, formal analysis; R.O. Anggaswara: investigation, formal analysis; M.L. Gunawan: writing-editing and review, resources, conceptualization, supervision, funding acquisition; G.T.M. Kadja: writing- editing and review, resources, conceptualization and supervision; I.G.B.N. Makertihartha: writing-editing and review, resources, conceptualization, methodology, funding acquisition, supervision. All authors have read and agreed to the published version of the manuscript.

References

[1] Holechek, J.L., Geli, H.M.E., Sawalhah, M.N., Valdez, R. (2022). A Global Assessment: Can Renewable Energy Replace Fossil Fuels by 2050?, *Sustainability (Switzerland)*, 14(8), 1–22. DOI: 10.3390/su14084792.

[2] MEMR (2023). Handbook of Energy & Economic Statistics of Indonesia. Jakarta: Ministry of Energy and Mineral Resources.

[3] Khande, A.R., Dasila, P.K., Majumder, S., Maity, P., Thota, C. (2021). Recent Developments in FCC Process and Catalysts. In: Pant, K.K., Gupta, S.K., Ahmad, E. (eds) *Catalysis for Clean Energy and Environmental Sustainability: Petrochemicals and Refining Process*es - Volume 2. Cham: Springer International Publishing, pp. 65–108. DOI: 10.1007/978-3-030-65021-6_3.

[4] Ross, J.R.H. (2019). Chapter 10 - Catalysis in the Production of Energy Carriers From Oil. In: Ross, J.R.H. (ed) *Contemporary Catalysis*. Amsterdam: Elsevier, pp. 233–249. DOI: https://doi.org/10.1016/B978-0-444-63474-0.00010-2.

[5] Sadeghbeigi, R. (2020). Chapter 5 - FCC catalysts. In: *Fluid Catalytic Cracking Handbook* (Fourth Edition), Fourth Edi. Butterworth-Heinemann, pp. 83–110. DOI: https://doi.org/10.1016/B978-0-12-812663-9.00005-9.

[6] Vogt, E.T.C., Whiting, G.T., Dutta Chowdhury, A., Weckhuysen, B.M. (2015). Chapter Two - *Zeolites and Zeotypes for Oil and Gas Conversion*. In: Jentoft, F.C. (ed). Academic Press, pp. 143–314.DOI: https://doi.org/10.1016/bs.acat.2015.10.001.

[7] Scherzer, J. (1993). Chapter 5 Correlation Between Catalyst Formulation and Catalytic Properties. In: Magee, J.S., Mitchell, M.M. (eds) *Fluid Catalytic Cracking: Science and Technology*. Elsevier, pp. 145–182.DOI: https://doi.org/10.1016/S0167-2991(08)63828-8.

[8] Feng, R., Qiao, K., Wang, Y., Yan, Z. (2013). Perspective on FCC catalyst in China. *Applied Petrochemical Research*, 3(3–4), 63–70. DOI: 10.1007/s13203-013-0030-1.

[9] Lloyd, L. (2011). Catalytic Cracking Catalysts. In: *Handbook of Industrial Catalysts*. Boston, MA: Springer US, pp. 169–210.DOI: 10.1007/978-0-387-49962-8_5.

[10] Gunawan, M.L., Rasrendra, C.B., Widikrama, C.L., Kurniawan, R.G., Nisa, L.M., Hudaya, F.Y.P., Makertihartha, I.G.B.N., Subagjo (2024). Investigation of the Effect of Silica and Phosphorus Content on the Performance of Active Matrix as Component of Cracking Catalyst. *Journal of Engineering and Technological Sciences*, 56(2), 205–218. DOI: 10.5614/j.eng.technol.sci.2024.56.2.3.

[11] Chen, S., Li, T., Cao, G., Guan, M. (2004). Amorphous silica-alumina, a carrier combination and a hydrocracking catalyst containing the same, and processes for the preparation thereof, *US Patent 6723297 B2*.

[12] Locus, R., Verboekend, D., d'Halluin, M., Dusselier, M., Liao, Y., Nuttens, N., Jaumann, T., Oswald, S., Mafra, L., Giebeler, L., Sels, B. (2018). Synthetic and Catalytic Potential of Amorphous Mesoporous Aluminosilicates Prepared by Postsynthetic Aluminations of Silica in Aqueous Media. *ChemCatChem*, 10(6), 1385–1397. DOI: 10.1002/cctc.201701660.

[13] Qoniah, I., Prasetyoko, D., Bahruji, H., Triwahyono, S., Jalil, A.A., Suprapto, Hartati, Purbaningtias, T.E. (2015). Direct synthesis of mesoporous aluminosilicates from Indonesian kaolin clay without calcination. *Applied Clay Science*, 118, 290–294. DOI: 10.1016/j.clay.2015.10.007.

[14] Twaiq, F.A., Mohamed, A.R., Bhatia, S. (2003). Liquid hydrocarbon fuels from palm oil by catalytic cracking over aluminosilicate mesoporous catalysts with various Si/Al ratios. *Microporous and Mesoporous Materials*, 64(1), 95–107. DOI: 10.1016/j.micromeso.2003.06.001.

[15] Xie, M., Li, Y., Etim, U.J., Lou, H., Xing, W., Wu, P., Liu, X., Bai, P., Yan, Z. (2019). Enhanced Catalytic Performance of the FCC Catalyst with an Alumina Matrix Modified by the Zeolite Y Structure-Directing Agent. *Industrial & Engineering Chemistry Research*, 58(14), 5455–5463. DOI: 10.1021/acs.iecr.8b04890.

[16] Souza, E.C. de, Pereira, M.M., Lam, Y.L., Morgado, E., Chinelatto, L.S. (2021). Aluminum phosphate as active matrix of fluid catalytic cracking catalysts: Y zeolite stabilization. *Applied Catalysis A: General*, 619(March), 118156. DOI: 10.1016/j.apcata.2021.118156.

[17] Hosseinpour, N., Mortazavi, Y., Bazyari, A., Khodadadi, A.A. (2009). Synergetic effects of Y-zeolite and amorphous silica-alumina as main FCC catalyst components on triisopropylbenzene cracking and coke formation. *Fuel Processing Technology*, 90(2), 171–179. DOI: 10.1016/j.fuproc.2008.08.013.

[18] Puspitasari, E. (2022). Development of Silica-Alumina Active Matrix with Addition of Phosphorus Compounds and Polyethylene Glycol (PEG) as Components of the Cracking Catalyst. *Master Thesis,* Bandung Institute of Technology.

[19] Sotomayor, F., Quantatec, A.P., Sotomayor, F.J., Cychosz, K.A., Thommes, M. (2018). Characterization of Micro/Mesoporous Materials by Physisorption: Concepts and Case Studies. *Acc. Mater. Surf. Res.*, 3(2), 34–50.

[20] Leofanti, G., Padovan, M., Tozzola, G., Venturelli, B. (1998). Surface area and pore texture of catalysts. *Catalysis Today*, 41(1), 207–219. DOI: 10.1016/S0920-5861(98)00050-9.

[21] Thommes, M., Kaneko, K., Neimark, A. V., Olivier, J.P., Rodriguez-Reinoso, F., Rouquerol, J., Sing, K.S.W. (2015). Physisorption of gases, with special reference to the evaluation of surface area and pore size distribution (IUPAC Technical Report). *Pure and Applied Chemistry*, 87(9–10), 1051–1069. DOI: 10.1515/pac-2014-1117.

[22] Cychosz, K.A., Thommes, M. (2018). Progress in the Physisorption Characterization of Nanoporous Gas Storage Materials. *Engineering*, 4(4), 559–566. DOI: 10.1016/j.eng.2018.06.001.

[23] Vogt, E.T.C., Weckhuysen, B.M. (2015). Fluid catalytic cracking: recent developments on the grand old lady of zeolite catalysis. *Chemical Society Reviews*, 44(20), 7342–7370. DOI: 10.1039/c5cs00376h.

[24] Asghari, A., Khorrami, M.K., Kazemi, S.H. (2019). Hierarchical H-ZSM5 zeolites based on natural kaolinite as a high-performance catalyst for methanol to aromatic hydrocarbons conversion. *Scientific Reports*, 9(1), 1–9. DOI: 10.1038/s41598-019-54089-y.

[25] Jentoft, F.C. (2013). Solid Acids and Bases. In: *Comprehensive Inorganic Chemistry II*. Elsevier, pp. 205–230. DOI: 10.1016/B978-0-08-097774-4.00720-8.

[26] Elimbi, A., Tchakoute, H.K., Njopwouo, D. (2011). Effects of calcination temperature of kaolinite clays on the properties of geopolymer cements. *Construction and Building Materials*, 25(6), 2805–2812. DOI: 10.1016/j.conbuildmat.2010.12.055.

[27] Soleimani, M., Bassi, A., Margaritis, A. (2007). Biodesulfurization of refractory organic sulfur compounds in fossil fuels. *Biotechnology Advances*, 25(6), 570–596. DOI: 10.1016/j.biotechadv.2007.07.003.

[28] Finocchiaro, C., Barone, G., Mazzoleni, P., Leonelli, C., Gharzouni, A., Rossignol, S. (2020). FT-IR study of early stages of alkali activated materials based on pyroclastic deposits (Mt. Etna, Sicily, Italy) using two different alkaline solutions. *Construction and Building Materials*, 262, 120095. DOI: 10.1016/j.conbuildmat.2020.120095.

[29] Rees, C.A., Provis, J.L., Lukey, G.C., van Deventer, J.S.J. (2007). In Situ ATR-FTIR Study of the Early Stages of Fly Ash Geopolymer Gel Formation. *Langmuir*, 23(17), 9076–9082. DOI: 10.1021/la701185g.

[30] Kubatová, D., Rybová, A., Zezulová, A., Švec, J. (2018). Thermal behaviour of inorganic aluminosilicate polymer based on cement kiln dust. *IOP Conference Series: Materials Science and Engineering*, 379(1) DOI: 10.1088/1757-899X/379/1/012008.

[31] Chimupala, Y., Junploy, P., Hardcastle, T., Westwood, A., Scott, A., Johnson, B., Brydson, R. (2016). Universal synthesis method for mixed phase TiO_2(B)/anatase TiO_2 thin films on substrates via a modified low pressure chemical vapour deposition (LPCVD) route. *Journal of Materials Chemistry A*, 4(15), 5685–5699. DOI: 10.1039/c6ta01383j.

[32] Rickard, W.D.A., Riessen, A. van, Walls, P. (2010). Thermal Character of Geopolymers Synthesized from Class F Fly Ash Containing High Concentrations of Iron and α-Quartz. *International Journal of Applied Ceramic Technology*, 7(1), 81–88. DOI: 10.1111/j.1744-7402.2008.02328.x.

[33] Vágvölgyi, V., Palmer, S.J., Kristóf, J., Frost, R.L., Horváth, E. (2008). Mechanism for hydrotalcite decomposition: A controlled rate thermal analysis study. *Journal of Colloid and Interface Science*, 318(2), 302–308. DOI: 10.1016/j.jcis.2007.10.033.

[34] Faqir, N.M., Shawabkeh, R., Al-Harthi, M., Wahhab, H.A. (2019). Fabrication of Geopolymers from Untreated Kaolin Clay for Construction Purposes. *Geotechnical and Geological Engineering*, 37(1), 129–137. DOI: 10.1007/s10706-018-0597-5.

[35] Zhang, Y.J., Wang, Y.C., Xu, D.L., Li, S. (2010). Mechanical performance and hydration mechanism of geopolymer composite reinforced by resin. *Materials Science and Engineering: A*, 527(24–25), 6574–6580. DOI: 10.1016/j.msea.2010.06.069.

[36] van der Bij, H.E., Weckhuysen, B.M. (2015). Phosphorus promotion and poisoning in zeolite-based materials: synthesis, characterisation and catalysis. *Chem. Soc. Rev.*, 44(20), 7406–7428. DOI: 10.1039/C5CS00109A.

[37] Abreu, J.S., Costa, L.M., Ferreira, L.D.L., de Oliveira, R.K.F.G., de Souza, T. da C.C., Nunes, E.H.M., Houmard, M. (2023). Hydrothermal treatment as a tool to tailor the mesoporous structure of sol-gel silica. *Journal of Non-Crystalline Solids*, 610(January), 122323. DOI: 10.1016/j.jnoncrysol.2023.122323.

[38] Kanezashi, M., Hataoka, N., Ikram, R., Nagasawa, H., Tsuru, T. (2021). Hydrothermal stability of fluorine-induced microporous silica membranes: Effect of steam treatment conditions. *AIChE Journal*, 67(9), 1–11. DOI: 10.1002/aic.17292.

[39] Fernandes, F.R.D., Pinto, F.G.H.S., Lima, E.L.F., Souza, L.D., Caldeira, V.P.S., Santos, A.G.D. (2018). Influence of synthesis parameters in obtaining KIT-6 mesoporous material. *Applied Sciences (Switzerland)*, 8(5), 725. DOI: 10.3390/app8050725.

[40] Khatrin, I., Kusuma, R.H., Kadja, G.T.M., Krisnandi, Y.K. (2023). Significance of ZSM-5 hierarchical structure on catalytic cracking: Intra- vs inter-crystalline mesoporosity. *Inorganic Chemistry Communications*, 149(October 2022), 110447. DOI: 10.1016/j.inoche.2023.110447.

[41] Williams, B.A., Babitz, S.M., Miller, J.T., Snurr, R.Q., Kung, H.H. (1999). The roles of acid strength and pore diffusion in the enhanced cracking activity of steamed Y zeolites. *Applied Catalysis A: General*, 177(2), 161–175. DOI: https://doi.org/10.1016/S0926-860X(98)00264-6.

[42] Corma, A., Corresa, E., Mathieu, Y., Sauvanaud, L., Al-Bogami, S., Al-Ghrami, M.S., Bourane, A. (2017). Crude oil to chemicals: light olefins from crude oil. *Catalysis Science & Technology*, 7(1), 12–46. DOI: 10.1039/C6CY01886F.

[43] Kadja, G.T.M., Azhari, N.J., Apriadi, F., Novita, T.H., Safira, I.R., Rasrendra, C.B. (2023). Low-temperature synthesis of three-pore system hierarchical ZSM-5 zeolite for converting palm oil to high octane green gasoline. *Microporous and Mesoporous Materials*, 360, 112731. DOI: 10.1016/j.micromeso.2023.112731

[44] Takahashi, R., Sato, S., Sodesawa, T., Goto, T., Matsutani, K., Mikami, N. (2007). Bending strength of silica gel with bimodal pores. II. Effect of variations in morphology and porosity. *Materials Research Bulletin*, 42(3), 523–531. DOI: 10.1016/j.materresbull.2006.06.015.

[45] Hezel, R., Ziegler, R. (1993). Correlation Between Catalyst Formulation and Catalytic Properties. *Solar Energy*, 76(December 1992), 260–264.

[46] Ishihara, A., Wakamatsu, T., Nasu, H., Hashimoto, T. (2014). Preparation of amorphous silica-alumina using polyethylene glycol and its role for matrix in catalytic cracking of n-dodecane. *Applied Catalysis A: General*, 478, 58–65. DOI: 10.1016/j.apcata.2014.03.016.

[47] Kadja, G.T.M., Ilmi, M.M., Azhari, N.J., Khalil, M., Fajar, A.T.N., Subagjo, Makertihartha, I.G.B.N., Gunawan, M.L., Rasrendra, C.B., Wenten, I.G. (2022). Recent advances on the nanoporous catalysts for the generation of renewable fuels. *Journal of Materials Research and Technology*, 17, 3277–3336. DOI: 10.1016/j.jmrt.2022.02.033.

[48] Makertihartha, I.G.B.N., Kadja, G.T.M., Gunawan, M.L., Mukti, R.R., Subagjo (2020). Exceptional aromatic distribution in the conversion of palm-oil to biohydrocarbon using zeolite-based catalyst. *Journal of Engineering and Technological Sciences*, 52(4), 584–597. DOI: 10.5614/j.eng.technol.sci.2020.52.4.9